Supplementary Materials for

Atom-by-atom assembly of defect-free one-dimensional cold atom arrays

Manuel Endres,* Hannes Bernien, Alexander Keesling, Harry Levine,
Eric R. Anschuetz, Alexandre Krajenbrink, Crystal Senko,
Vladan Vuletic, Markus Greiner, Mikhail D. Lukin

*Corresponding author. Email: mendres@caltech.edu

This PDF file includes:

Materials and Methods
Figs. S1 to S5
References

Other Supplementary Material for this manuscript includes the following:
(available at www.sciencemag.org/cgi/content/full/science.aah3752/DC1)

Movies S1 to S3

Supplementary Information:
Atom-by-atom assembly of defect-free one-dimensional cold atom arrays

Manuel Endres,[1, 2, *] Hannes Bernien,[1, *] Alexander Keesling,[1, *] Harry Levine,[1, *] Eric R. Anschuetz,[1]
Alexandre Krajenbrink,[1, †] Crystal Senko,[1] Vladan Vuletic,[3] Markus Greiner,[1] and Mikhail D. Lukin[1]

[1] *Department of Physics, Harvard University, Cambridge, MA 02138, USA*
[2] *Division of Physics, Mathematics and Astronomy, California Institute of Technology, Pasadena, CA 91125, USA*
[3] *Department of Physics and Research Laboratory of Electronics,*
Massachusetts Institute of Technology, Cambridge, MA 02139, USA

CONTENTS

1 EXPERIMENTAL SEQUENCE

1.1 Trap loading

We use an external-cavity diode laser at ≈ 809 nm to seed a tapered amplifier (Moglabs, MOA002), which provides 1.8 W of output power. The resulting beam is coupled into a single-mode fiber, and passed through three laser clean-up filters (Semrock LL01-808). This results in a 4 mm beam with ≈ 550 mW of power, which is split into an array of beams by an acousto-optic deflector (AOD) (AA Opto-Electronic model DTSX-400-800.850). These beams pass through a 1:1 telescope with 300 mm focal length and are then focused by a 0.5 NA microscope objective (Mitutoyo G Plan Apo 50X) into our vacuum chamber to form an array of optical tweezers (Fig. 1B of the main text). These tweezers have a waist of ≈ 900 nm, and their centers are separated by $2.6\,\mu$m. Each beam has ≈ 1 mW of optical power, corresponding to a trap depth of ≈ 0.9 mK for ^{87}Rb atoms.

The experimental sequence begins by laser cooling thermal ^{87}Rb atoms in a magneto-optical trap (MOT) around the traps for 100 ms (Fig. S1A). We use a gradient field of 9.7 G/cm, and three intersecting retroreflected beams that are 17 MHz red detuned of the free space $F = 2 \rightarrow F' = 3$ transition, overlapped with repumper beams resonant with the free space $F = 1 \rightarrow F' = 2$ transition. One of these beams is perpendicular to the optical table, and the other two

---

* These authors contributed equally to this work.
† Current address: CNRS-Laboratoire de Physique Théorique de l'Ecole Normale Supérieure, 24 rue L'homond, 75231 Paris Cedex, France
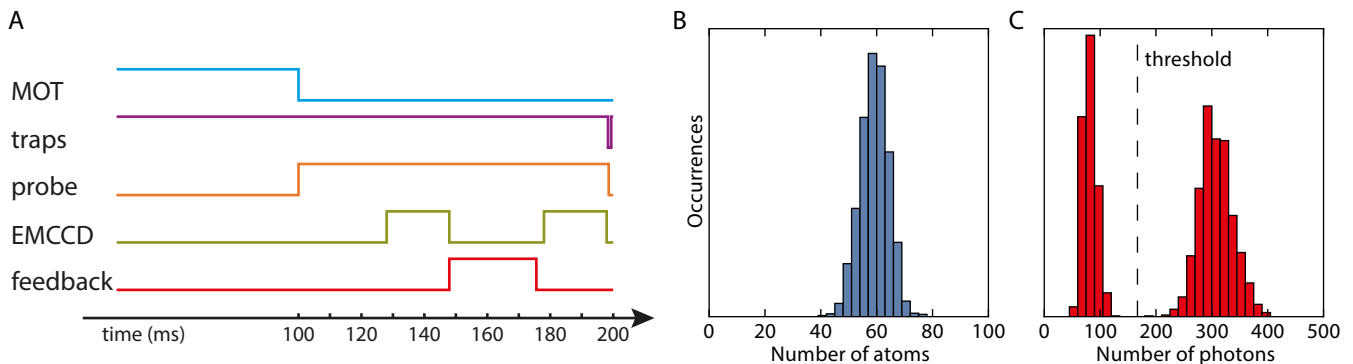
Figure S1. **Experimental sequence and atomic signal. A)** Pulse diagram of the experimental sequence. **B)** Distribution of number of initially loaded atoms. **C)** Sample fluorescence count distribution for a single trap during 20 ms of exposure.

are parallel to it (intersecting at an angle of $\approx 120°$ due to the geometric restriction imposed by the high resolution objectives). All three beams have a diameter of ≈ 1.5 cm, and carry ≈ 1.5 mW of cooling light and ≈ 0.4 mW of repumping light each. To reduce the necessary time to load the MOT, we shine UV light from a diode at 365 nm directly on the region of the glass cell within which the MOT is loaded [40].

After 100 ms, the magnetic field gradient and the MOT beams are turned off to allow the MOT to dissipate over 28 ms. At the same time we turn on a set of probe beams which are 20 MHz red-detuned from the bare atom $F = 2 \to F' = 3$ transition. The probe beams have the same geometric configuration as the MOT beams, but they have ≈ 50 times less power, and a diameter of ≈ 1 mm, which largely reduces background light due to stray reflections during imaging. The probe beams further cool the atoms through polarization-gradient cooling, and are left on for the remainder of the sequence.

The result of this process is the probabilistic loading of atoms into the traps. For the data presented in Fig. 3 of the main text we loaded on average 59±5 atoms (Fig. S1B).

1.2 Imaging

The EMCCD camera (Andor iXON3) is triggered 128 ms after the beginning of the experimental sequence and acquires an image over the following 20 ms. Cooling light from the probe beams is scattered by the atoms and collected on the EMCCD, forming an image of the atoms in the array. Based on the collected photon statistics for each trap, we can set clear thresholds to determine the presence of an atom in a trap (see Fig. S1C). Furthermore, the bimodal nature of the photon statistics is an indication that the traps are occupied by either 0 or 1 atom.

1.3 Feedback

Once the EMCCD has finished acquiring the signal, the image file is transferred over the following 10 ms to a computer which determines trap occupations, using pre-calibrated regions of interest and threshold counts for each trap, in sub-ms time. Using this information, the computer finds the correct pre-calculated waveform to displace each occupied trap during 3 ms from its initial position to its final position, and then adds up all of them into a multi-tone frequency-sweep waveform. This computation takes ≈ 0.2 ms for each trap to be displaced. Once the waveform is ready, it is sent to the AOD to perform the trap displacement, and then it goes back to producing the original set of 100 traps. It is important to note that the rearrangement waveform is only calculated for loaded traps, which means that all empty traps are turned off for the duration of the rearrangement but are restored immediately afterwards, so that the trap array returns after rearrangement to its original configuration. After rearrangement, there is a ≈ 7 ms buffer time before taking another 20 ms exposure image with the EMCCD. The entire process, consisting of image acquisition, transfer, analysis, waveform generation, rearrangement, and buffer, takes a total of 50 ms.

Currently, the profile of the frequency sweeps is calculated to be piece-wise quadratic in time, over a duration of 3 ms. For shorter transport times we observe an increase in the number of atoms lost during rearrangement. For the experiments reported in the main text, atom losses are only slightly increased compared to the expected lifetime in
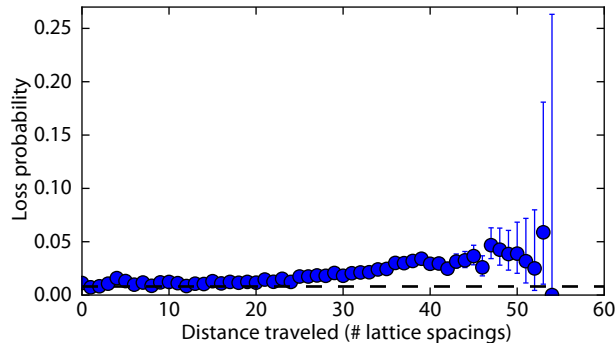
Figure S2. **Rearrangement losses.** Losses as a function of total distance traveled by the atom during rearrangement for the dataset presented in Fig. 3 of the main text. The dashed line represents the expected loss for a stationary trap with 6.2 s lifetime.

static traps (see Fig. S2). These losses depend on the distance that the atoms move, and it is possible that they could be reduced by changing the length or the profile of the frequency sweep to minimize acceleration and jerk during the trajectory. However, the fidelity of our rearrangement would not be significantly improved by minimizing these losses (see Fig. 3B of the main text).

2 EXPERIMENTAL METHODS

2.1 Generating 100 traps

When driving the AOD with a single radio frequency (RF) tone, a portion of the input beam is deflected by an angle θ that depends on the frequency ω of the tone. By applying 100 different RF tones $\{\omega_1, \ldots, \omega_{100}\}$, we generate 100 beams with output angles $\{\theta_1, \ldots, \theta_{100}\}$, where $\theta_i = \theta(\omega_i)$. The waveform that we send into the AOD is initially calculated by a computer that samples the desired waveform in the time-domain with a sampling rate of 100 MHz. We stream these waveform samples to a Software Defined Radio (SDR) (Ettus Research, model USRP X310, daughterboard UBX 160) which performs digital-analog conversion, low-pass filtering, and subsequent analog IQ upconversion by a frequency of $\omega_{\mathrm{up}} = 74$ MHz, and outputs an analog waveform, which we then amplify and send to the AOD. The waveform that we calculate initially is given by:

$$\sum_{i=1}^{100} A_i e^{i\phi_i} e^{i(\omega_i - \omega_{\mathrm{up}})t},$$

with A_i and ϕ_i being the real amplitude and phase, respectively, of the RF tone with frequency ω_i. Since we generate all tones in the same waveform (relative to the same local oscillator inside the SDR), the tones in our waveform have well-defined phases $\{\phi_i\}$ relative to one another. Also, since all the frequencies we use are integer multiples of 1 kHz, we calculate a 1 ms waveform which is streamed on a loop without needing to continuously generate new samples.

2.2 Effects of intermodulation

The finite power bandwidth, along with other imperfections of our system (RF amplifier and AOD) generate a nonlinear response to the input signal. To the lowest order nonlinearity, the system acts as a mixer and generates new tones at the sum and difference of the input frequencies. For example, for two tones, $A_1 e^{i\phi_1} e^{i\omega_1 t}$, $A_2 e^{i\phi_2} e^{i\omega_2 t}$, at the input, there will be a corresponding set of tones at the output:

$$E_{1,2}^{-} \propto e^{i(\phi_1 - \phi_2)} e^{i(\omega_1 - \omega_2)t},$$

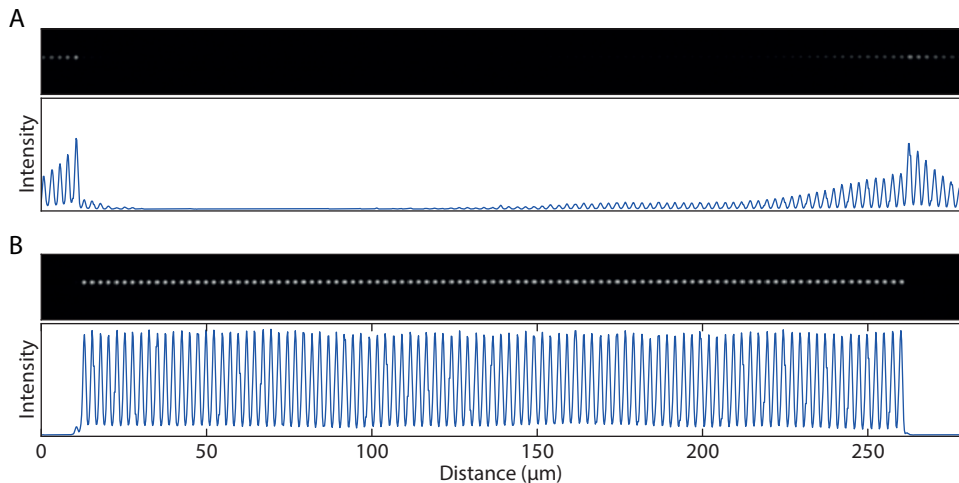$$E_{1,2}^{+} \propto e^{i(\phi_1 + \phi_2)} e^{i(\omega_1 + \omega_2)t}$$

Figure S3. **Generating uniform traps.** Nonlinearities inside the AOD and RF amplifier cause frequency mixing. (**A**) Setting identical phases for each input tone results in intermodulations that strongly interfere with the intended frequency tones and significantly distort the trap amplitudes. (**B**) By optimizing the phases $\{\phi_i\}$ and amplitudes $\{A_i\}$ of the RF tones we can reduce intermodulations and generate homogeneous traps.

These terms are far removed from the main set of desired tones $\{\omega_i\}$ and can in principle be filtered by frequency. However, they seed the next order of nonlinearity.

The next order of nonlinearity contains the mixing of these first order nonlinearities with the original tones. For example, with two tones we would now see a mixing of the $(\omega_1 - \omega_2)$ tone with the original ω_1 tone to produce a sum tone at $(2\omega_1 - \omega_2)$ and a difference tone at ω_2. Similarly, the $(\omega_1 - \omega_2)$ tone would mix with the original ω_2 tone to produce a tone at $(2\omega_2 - \omega_1)$ and ω_1. If the phases of each input tone $\{\phi_i\}$ are not carefully selected, these intermodulations interfere destructively with the original tones, as shown in Fig. S3A.

2.3 Optimizing trap homogeneity

We address the issue of intermodulations by adjusting the phases of the different RF tones to almost completely cancel out the nonlinearities. As a first step, we generate a computer simulation of 100 tones evenly spaced in frequency and with random phases, and equal amplitudes. For each pair of traps $\{i, j\}$, we calculate the difference tone $E^-_{i,j}$. By starting with random initial phases, the difference tones nearly completely destructively interfere with one another. We then optimize each phase, one at a time, to further reduce the sum of all difference tones $\sum E^-_{i,j}$. After this, we proceed to generate the waveform to be streamed onto the SDR. The starting amplitudes for each tone are selected such that they individually produce a single deflection carrying the correct amount of optical power. The frequencies span from 74.5 MHz to 123.01 MHz in steps of 0.49 MHz.

The next step in optimization consists of imaging the focused trap array on a CCD and performing 2D Gaussian fits. We use the amplitude of these fits to feed back on the amplitude of the individual tones. Once all the fitted amplitudes are approximately uniform, we continue to the last step of optimization.

Since we are interested in the uniformity of the traps at the positions of the atoms, we measure the AC Stark shifts induced by the traps, and use these values to feed back on the amplitude of each tone. In order to extract the AC Stark shift, we shine a single laser beam onto the trapped atoms for $10\,\mu$s, and measure the loss probability introduced by this "pushout" beam as a function of detuning from the bare $F = 2 \rightarrow F' = 3$ resonance (Fig. S4A inset). From the fits we extract the individual lightshift for each trap and use these values to perform feedback on the amplitudes. We repeat the procedure until the shifted resonances are uniform to within $\approx 2\%$ across the trap array (Fig. S4A). At this point we have a set of optimal amplitudes $\{A_i^{opt}\}$ and phases $\{\phi_i^{opt}\}$ associated with the RF frequencies $\{\omega_i\}$ (Fig. S3B). We interpolate between the values of $\{A_i^{opt}\}$ to define the optimal amplitude as a function of frequency $A^{opt}(\omega)$.
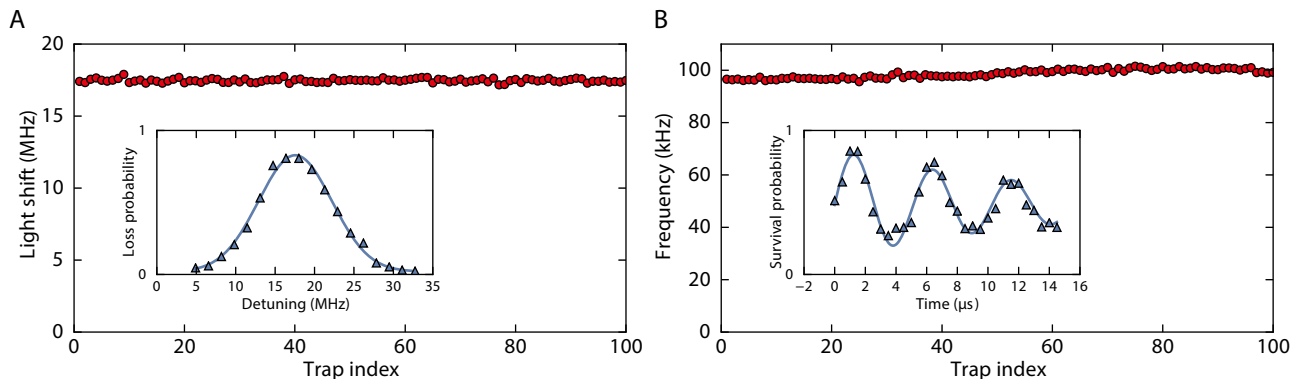
Figure S4. **Characterization of trap and atom properties.** (**A**) The trapping light causes a lightshift on the atomic resonances that depends on the amplitude of the trap. The measured lightshifts across the array are used to optimize the RF amplitudes $\{A_i\}$. This process results in homogeneous traps with lightshifts that are uniform to within $\approx 2\%$. Inset shows the result of a pushout measurement (see text) on trap 26 that is used to determine the individual lightshift. (**B**) The trap frequencies are determined from a release and recapture measurement [41] (see inset for trap 26). The errors from the fits are smaller than the marker size for all the figures.

2.4 Characterizing trap homogeneity

To characterize the homogeneity of the final trap configuration, we perform experiments to determine the AC Stark shift and trap frequency for each trap in the array (Fig. S4).

As outlined in the previous section, the measurement of the AC Stark shift is used to equalize the traps. We find an average shift of 17.5 MHz with a standard deviation of 0.1 MHz across the whole array.

The trap frequency (Fig. S4B) is found through a release and recapture technique [41]. We obtain the radial frequency from a fit to the probability of retaining an atom as a function of hold time (Fig. S4B inset). We find the average trap frequency to be 98.7 kHz with a standard deviation of 1.7 kHz across the array. Combining these measurements with an independent determination of the waist, we estimate a trap depth of ≈ 0.9 mK.

2.5 Moving traps

For most of the experimental sequence time, the traps are static. However, during short bursts we stream new waveforms to the AOD to rearrange them, and the atoms they hold. We move our traps by sweeping the frequencies $\{\omega_i(t)\}$ of the tones that correspond to the traps we wish to move, in a piecewise-quadratic fashion. This way, the atoms experience a constant acceleration a for the first half of the trajectory, and $-a$ for the second half. During the sweep, we also continuously adjust the amplitude of the RF tone to match the optimized amplitude for its current frequency: $A_i(t) = A^{opt}(\omega_i(t))$. Further, by slightly adjusting the duration of each sweep, we enforce each trap to end with the optimal phase corresponding to its new position.

Using these parameters we pre-calculate all waveforms to sweep the frequency of a tone at any given starting frequency in our array to any given final frequency, over 3 ms. This amounts to 100^2 precalculated trajectories.

2.6 Lifetimes

The lifetime for each trap is found by an exponential fit to the probability of retaining an atom as a function of time. Under optimal conditions, this results in an average lifetime for the traps in our array of 11.6 s with a standard deviation of 0.5 s across the array. However, this value depends on the background pressure inside the vacuum chamber and therefore depends on the current with which we drive our dispenser atom source. For the measurements presented in Fig. 3 of the main text, an average lifetime of 6.2 s was found from independent calibration measurements.

In these measurements, we apply continuous laser cooling throughout the hold time. We observe that without continuous cooling, the lifetime is reduced compared to these values. The retention as a function of time in this case does not follow a simple exponential decay (indicative of a heating process), and we define the time at which the

retention probability crosses $1/e$ to be the lifetime. For the standard configuration in the main text (100 traps with 0.49 MHz spacing between neighboring frequencies), we find a lifetime of ≈ 0.4 s. While we have not characterized the source of the lifetime reduction in detail, we have carried out a number of measurements in different configurations to distinguish various effects:

- Generating a single trap by driving the AOD with a single frequency from a high-quality signal generator (Rohde & Schwarz SMC100A), we find a lifetime of ≈ 2 s. This indicates that there are additional heating effects, such as photon scattering from trap light or intensity noise, that are independent of the use of the SDR or the fact that we drive the AOD with a large number of frequencies. Possible improvements include using further detuned trap light and improving our intensity stabilization. Furthermore, in a separate experiment [35], we observed that using a Titanium-Sapphire laser instead of a TA significantly improved trap lifetimes even at the same trapping wavelength.

- Generating a single trap by driving the AOD with a single frequency from the SDR, we find a lifetime of ≈ 1 s. This indicates that the RF-waveforms from the SDR could have additional phase or intensity noise. A possible source is the local oscillator used for IQ upconversion in the SDR, which could be replaced with a more phase-stable version.

- We observe the same trap lifetime of ≈ 1 s when driving the AOD with 70 frequencies at a spacing of 0.7 MHz using the SDR. This indicates that, in principle, there is no lifetime reduction associated with driving the AOD with a large number of frequencies.

- We observe a reduction of lifetime for frequency spacings smaller than ≈ 0.65 MHz. For example, we found a lifetime of ≈ 0.4 s, when setting the frequency spacing to 0.49 MHz. (This lifetime is unchanged by increasing the number of traps from 70 to 100.) We interpret this effect to be the result of interference between neighboring traps. Due to the finite spatial overlap of the tweezer light, a time-dependent modulation occurs with a frequency given by the frequency spacing between neighboring traps. When bringing traps closer together, both the spatial overlap increases and the modulation frequency approaches the parametric heating resonance at ≈ 200kHz given by twice the radial trapping frequency.

We would like to stress that these effects only play a role after the rearrangement procedure is completed. During rearrangement, continuous laser cooling is a valid and powerful method to reduce heating effects. Additionally, the flexibility of our system makes it possible to load and continuously cool atoms in a set of closely spaced traps, and to rearrange the filled traps to an array with larger separations, at which point cooling can be turned off. This method of rearrangement takes advantage of the large number of atoms that can be initially loaded in our set of 100 traps separated by 0.49 MHz, while eliminating the effect of interference by setting a larger final frequency separation of, for example, 0.7 MHz. Furthermore, atoms could also be transferred into a fully "static" trap array, such as an optical lattice, after rearrangement.

However, even with optimal cooling parameters, heating effects cannot be always compensated. For example, we observed a significant reduction of lifetime for frequency spacings below ≈ 0.45 MHz even with continuous laser cooling. This sets a limit on the maximum number of traps that can be generated within the bandwitdh of our AOD, and therefore limits the final sizes of the atomic arrays.

3 PROSPECTS FOR EXTENSIONS TO 2D ARRAYS

In this section we will discuss possible extensions of our method to form uniformly filled two-dimensional (2d) arrays. We will describe two different rearrangement strategies and compare their performance given realistic parameters for loading efficiencies and lifetimes.

3.1 Method 1: Row or column deletion and rearrangement

Using a 2d AOD we could generate a 2d array of optical tweezers using two sets of RF tones, one set corresponding to rows and the other corresponding to columns. After loading atoms probabilistically into the array, it would be possible to eliminate each defect by turning off the RF frequency that generates either the row or the column containing the defect, and then transport all remaining rows and columns to form a defect-free uniform array.
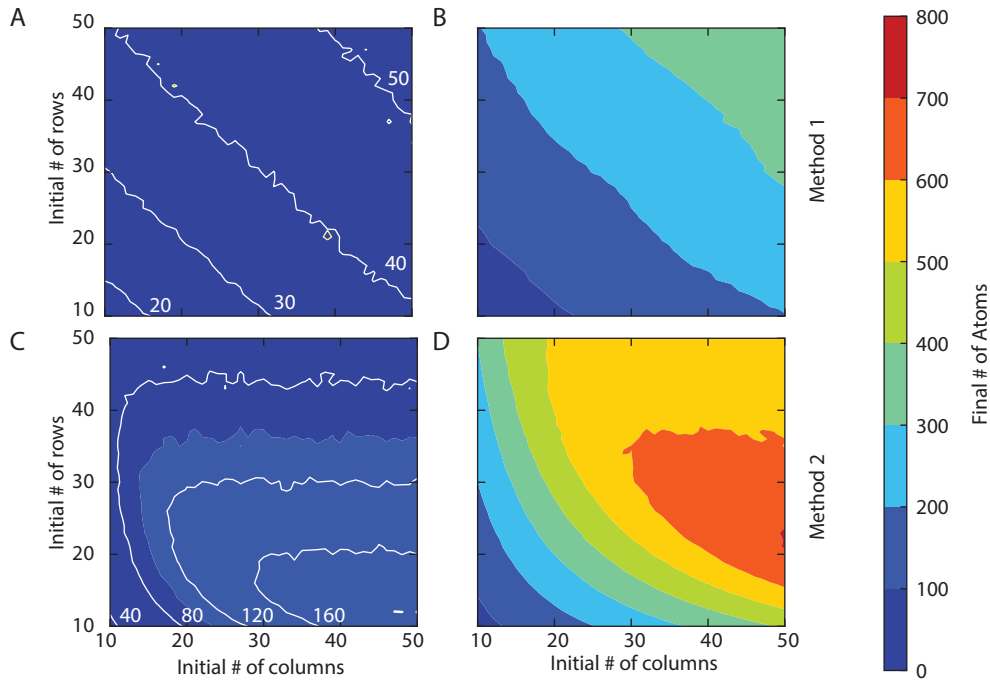
Figure S5. **Projections for 2D system sizes.** Expected number of atoms in defect free rectangular arrays generated through the "Row or column deletion and rearrangement method" with 0.6 loading efficiency and 10 s lifetime (**A**), and with 0.9 loading efficiency and 60 s lifetime (**B**). Expected number of atoms in defect free rectangular arrays generated through the "Row-by-row rearrangement method" with 0.6 loading efficiency and 10 s lifetime (**C**), and with 0.9 loading efficiency and 60 s lifetime (**D**).

3.2 Method 2: Row-by-row rearrangement

A different approach is to generate a static two-dimensional array of traps using techniques such as optical lattices or spatial-light modulators. In a first step, atoms would be probabilistically loaded into this static array. After loading, we could use an independent AOD to generate a linear array of traps, deeper than the ones forming the static array and overlapping precisely with one row of static traps. By rearranging the linear array, we could transfer the atoms to their final locations in the static configuration, where they would remain after turning off the traps used for transport. Doing this for each row would make it possible to fill an entire region of the static 2d array.

3.3 Expected performance and scalability

The final size of the array will depend on the initial loading efficiency, while the probability to have a defect-free array after rearrangement will depend on the atom lifetimes in the traps, and the total feedback time. This time consists of several blocks: image taking, image transfer, waveform calculation, and trap movement. We can take an image in 20 ms. The time it takes to transfer the image from the camera to the computer takes a minimum of 9 ms and each row of atoms adds 0.8 ms to the transfer time. Analyzing the image to determine the location of the atoms and necessary frequency sweeps can be done in sub-ms time. Generating the waveform takes ≈ 0.2 ms for each sweep necessary. This time scales as the final number of atoms ($O(N)$) for method 2, and with the final number of rows and columns ($O(N^{1/2})$) for method 1. Finally, the rearrangement itself takes 3 ms for each set of frequency sweeps: for method 1 there are two sweeps, and for method 2 the number of sweeps equals the number of rows.

Figure S5 shows the result of a Monte Carlo simulation for the expected number of atoms in a defect-free rectangular array using two sets of parameters, and both rearrangement methods described above. Given our current loading efficiency of 0.6 and vacuum-limited lifetime of ≈ 10 s, we can expect more than 160 atoms in the final defect-free configuration (Fig. S5A, C). However, if we were to upgrade our vacuum setup to increase the lifetime from 10 s to 60 s, and we increased the loading efficiency to 0.9 using currently available techniques [21,22,23], we could expect more than 600 atoms in defect-free configurations (Fig. S5B, D). These numbers were calculated by simulating a sequence that performed repeated rearrangement until no more defects appeared, and every point on the plot is the

average of 500 simulations.

4. MOVIES OF THE REARRANGEMENT PROCEDURES

VS1: Rearrangement procedure. This video shows consecutive pairs of atom fluorescence images. Each pair consists of an initial image showing the random loading into the array of traps and a subsequent image after the loaded atoms have been rearranged to form a regular array. The sequence of images demonstrates the effectiveness of the procedure to reduce the entropy associated with the random initial positions of the atoms by ordering them in long, uninterrupted chains. The 1 Hz cycle rate in the video is slowed down by a factor of five relative to the 5 Hz experimental repetition rate.

VS2: Lifetime extension of 20 atom array. This video shows consecutive fluorescence images of atoms being rearranged from an initial probabilistic loading into an ordered array of 20 atoms and a reservoir formed by surplus atoms. The length of the target array is kept constant by transporting atoms from the reservoir to replace lost atoms in the target array. This technique makes it possible to extend the average lifetime of a defect-free 20 atom array to ≈ 8 s, at which point the reservoir typically has depleted. The 10 Hz frame rate of this video accurately reflects the rate at which these images were acquired.

VS3: Lifetime extension of 40 atom array. This video shows consecutive fluorescence images of atoms being rearranged from an initial probabilistic loading into an ordered array of 40 atoms and a reservoir formed by surplus atoms. The length of the target array is kept constant by transporting atoms from the reservoir to replace lost atoms in the target array. This technique makes it possible to extend the average lifetime of a defect-free 40 atom array to ≈ 2 s, at which point the reservoir typically has depleted. The 10 Hz frame rate of this video accurately reflects the rate at which these images were acquired.

References

1. S. Haroche, Controlling photons in a box and exploring the quantum to classical boundary. *Ann. Phys.* **525**, 753–776 (2013). doi:10.1002/andp.201300737

2. D. J. Wineland, Nobel Lecture: Superposition, entanglement, and raising Schrödinger's cat. *Rev. Mod. Phys.* **85**, 1103–1114 (2013). doi:10.1103/RevModPhys.85.1103

3. C. Monroe, J. Kim, Scaling the ion trap quantum processor. *Science* **339**, 1164–1169 (2013). Medline doi:10.1126/science.1231298

4. M. H. Devoret, R. J. Schoelkopf, Superconducting circuits for quantum information: An outlook. *Science* **339**, 1169–1174 (2013). Medline doi:10.1126/science.1231930

5. W. S. Bakr, A. Peng, M. E. Tai, R. Ma, J. Simon, J. I. Gillen, S. Fölling, L. Pollet, M. Greiner, Probing the superfluid-to-Mott insulator transition at the single-atom level. *Science* **329**, 547–550 (2010). Medline doi:10.1126/science.1192368

6. J. F. Sherson, C. Weitenberg, M. Endres, M. Cheneau, I. Bloch, S. Kuhr, Single-atom-resolved fluorescence imaging of an atomic Mott insulator. *Nature* **467**, 68–72 (2010). Medline doi:10.1038/nature09378

7. C. Weitenberg, M. Endres, J. F. Sherson, M. Cheneau, P. Schauss, T. Fukuhara, I. Bloch, S. Kuhr, Single-spin addressing in an atomic Mott insulator. *Nature* **471**, 319–324 (2011). Medline doi:10.1038/nature09827

8. D. S. Weiss, J. Vala, A. V. Thapliyal, S. Myrgren, U. Vazirani, K. B. Whaley, Another way to approach zero entropy for a finite system of atoms. *Phys. Rev. A* **70**, 040302 (2004). doi:10.1103/PhysRevA.70.040302

9. J. Vala, A. V. Thapliyal, S. Myrgren, U. Vazirani, D. S. Weiss, K. B. Whaley, Perfect pattern formation of neutral atoms in an addressable optical lattice. *Phys. Rev. A* **71**, 032324 (2005). doi:10.1103/PhysRevA.71.032324

10. N. Schlosser, G. Reymond, I. Protsenko, P. Grangier, Sub-poissonian loading of single atoms in a microscopic dipole trap. *Nature* **411**, 1024–1027 (2001). Medline [doi:10.1038/35082512](doi:10.1038/35082512)

11. M. Weber, J. Volz, K. Saucke, C. Kurtsiefer, H. Weinfurter, Analysis of a single-atom dipole trap. *Phys. Rev. A* **73**, 043406 (2006). doi:10.1103/PhysRevA.73.043406

12. K. D. Nelson, X. Li, D. S. Weiss, Imaging single atoms in a three-dimensional array. *Nat. Phys.* **3**, 556–560 (2007). doi:10.1038/nphys645

13. M. J. Piotrowicz, M. Lichtman, K. Maller, G. Li, S. Zhang, L. Isenhower, M. Saffman, Two-dimensional lattice of blue-detuned atom traps using a projected Gaussian beam array. *Phys. Rev. A* **88**, 013420 (2013). doi:10.1103/PhysRevA.88.013420

14. F. Nogrette, H. Labuhn, S. Ravets, D. Barredo, L. Béguin, A. Vernier, T. Lahaye, A. Browaeys, Single-atom trapping in holographic 2D arrays of microtraps with arbitrary geometries. *Phys. Rev. X* **4**, 021034 (2014); http://journals.aps.org/prx/abstract/10.1103/PhysRevX.4.021034.

15. A. M. Kaufman, B. J. Lester, C. M. Reynolds, M. L. Wall, M. Foss-Feig, K. R. Hazzard, A. M. Rey, C. A. Regal, Two-particle quantum interference in tunnel-coupled optical tweezers. *Science* **345**, 306–309 (2014). Medline doi:10.1126/science.1250057

16. A. M. Kaufman, B. J. Lester, M. Foss-Feig, M. L. Wall, A. M. Rey, C. A. Regal, Entangling two transportable neutral atoms via local spin exchange. *Nature* **527**, 208–211 (2015). Medline doi:10.1038/nature16073

17. Y. Miroshnychenko, W. Alt, I. Dotsenko, L. Förster, M. Khudaverdyan, D. Meschede, D. Schrader, A. Rauschenbeutel, Quantum engineering: An atom-sorting machine. *Nature* **442**, 151 (2006). Medline doi:10.1038/442151a

18. J. Beugnon, C. Tuchendler, H. Marion, A. Gaëtan, Y. Miroshnychenko, Y. R. P. Sortais, A. M. Lance, M. P. A. Jones, G. Messin, A. Browaeys, P. Grangier, Two-dimensional transport and transfer of a single atomic qubit in optical tweezers. *Nat. Phys.* **3**, 696–699 (2007). doi:10.1038/nphys698

19. M. Schlosser, J. Kruse, C. Gierl, S. Teichmann, S. Tichelmann, G. Birkl, Fast transport, atom sample splitting and single-atom qubit supply in two-dimensional arrays of optical microtraps. *New J. Phys.* **14**, 123034 (2012). doi:10.1088/1367-2630/14/12/123034

20. H. Kim, W. Lee, H.-g. Lee, H. Jo, Y. Song, J. Ahn, In situ single-atom array synthesis using dynamic holographic optical tweezers. arXiv:1601.03833 (2016); https://arxiv.org/pdf/1601.03833.pdf.

21. T. Grünzweig, A. Hilliard, M. McGovern, M. F. Andersen, Near-deterministic preparation of a single atom in an optical microtrap. *Nat. Phys.* **6**, 951–954 (2010). doi:10.1038/nphys1778

22. B. J. Lester, N. Luick, A. M. Kaufman, C. M. Reynolds, C. A. Regal, Rapid production of uniformly filled arrays of neutral atoms. *Phys. Rev. Lett.* **115**, 073003 (2015). Medline doi:10.1103/PhysRevLett.115.073003

23. Y. H. Fung, M. F. Andersen, Efficient collisional blockade loading of a single atom into a tight microtrap. *New J. Phys.* **17**, 073011 (2015). doi:10.1088/1367-2630/17/7/073011

24. D. Jaksch, J. I. Cirac, P. Zoller, S. L. Rolston, R. Cote, M. D. Lukin, Fast quantum gates for neutral atoms. *Phys. Rev. Lett.* **85**, 2208–2211 (2000). Medline doi:10.1103/PhysRevLett.85.2208

25. M. Saffman, T. G. Walker, K. Mølmer, Quantum information with Rydberg atoms. *Rev. Mod. Phys.* **82**, 2313–2363 (2010). doi:10.1103/RevModPhys.82.2313

26. H. Weimer, M. Müller, I. Lesanovsky, P. Zoller, H. P. Büchler, A Rydberg quantum simulator. *Nat. Phys.* **6**, 382–388 (2010). doi:10.1038/nphys1614

27. A. Browaeys, D. Barredo, T. Lahaye, Experimental investigations of dipole-dipole interactions between a few Rydberg atoms. *J. Phys. B* **49**, 152001 (2016). doi:10.1088/0953-4075/49/15/152001

28. J. D. Thompson, T. G. Tiecke, N. P. de Leon, J. Feist, A. V. Akimov, M. Gullans, A. S. Zibrov, V. Vuletić, M. D. Lukin, Coupling a single trapped atom to a nanoscale optical cavity. *Science* **340**, 1202–1205 (2013). Medline doi:10.1126/science.1237125

29. A. Goban, C. L. Hung, S. P. Yu, J. D. Hood, J. A. Muniz, J. H. Lee, M. J. Martin, A. C. McClung, K. S. Choi, D. E. Chang, O. Painter, H. J. Kimble, Atom-light interactions in photonic crystals. *Nat. Commun.* **5**, 3808 (2014). Medline doi:10.1038/ncomms4808

30. S. Murmann, F. Deuretzbacher, G. Zürn, J. Bjerlin, S. M. Reimann, L. Santos, T. Lompe, S. Jochim, Antiferromagnetic Heisenberg spin chain of a few cold atoms in a one-dimensional trap. *Phys. Rev. Lett.* **115**, 215301 (2015). Medline doi:10.1103/PhysRevLett.115.215301

31. See supplementary materials on *Science* Online.

32. T. Xia, M. Lichtman, K. Maller, A. W. Carr, M. J. Piotrowicz, L. Isenhower, M. Saffman, Randomized benchmarking of single-qubit gates in a 2D array of neutral-atom qubits. *Phys. Rev. Lett.* **114**, 100503 (2015). Medline doi:10.1103/PhysRevLett.114.100503

33. Y. Wang, X. Zhang, T. A. Corcovilos, A. Kumar, D. S. Weiss, Coherent addressing of individual neutral atoms in a 3D optical lattice. *Phys. Rev. Lett.* **115**, 043003 (2015). Medline doi:10.1103/PhysRevLett.115.043003

34. A. M. Kaufman, B. J. Lester, C. A. Regal, Cooling a single atom in an optical tweezer to its quantum ground state. *Phys. Rev. X* **2**, 041014 (2012); http://journals.aps.org/prx/abstract/10.1103/PhysRevX.2.041014.

35. J. D. Thompson, T. G. Tiecke, A. S. Zibrov, V. Vuletić, M. D. Lukin, Coherence and Raman sideband cooling of a single atom in an optical tweezer. *Phys. Rev. Lett.* **110**, 133001 (2013). Medline doi:10.1103/PhysRevLett.110.133001

36. P. Kómár, T. Topcu, E. M. Kessler, A. Derevianko, V. Vuletić, J. Ye, M. D. Lukin, Quantum network of atom clocks: A possible implementation with neutral atoms. *Phys. Rev. Lett.* **117**, 060506 (2016). Medline doi:10.1103/PhysRevLett.117.060506

37. J. F. Barry, D. J. McCarron, E. B. Norrgard, M. H. Steinecker, D. DeMille, Magneto-optical trapping of a diatomic molecule. *Nature* **512**, 286–289 (2014). Medline doi:10.1038/nature13634

38. N. R. Hutzler, L. R. Liu, Y. Yu, K.-K. Ni, Eliminating light shifts in single-atom optical traps. arXiv:1605.09422 (2016); https://arxiv.org/abs/1605.09422.

39. D. Barredo, S. de Léséleuc, V. Lienhard, T. Lahaye, A. Browaeys, An atom-by-atom assembler of defect-free arbitrary 2d atomic arrays. arXiv: 1607.03042; https://arxiv.org/abs/1607.03042

40. C. Klempt, T. van Zoest, T. Henninger, O. Topic, E. Rasel, W. Ertmer, J. Arlt, Ultraviolet light-induced atom desorption for large rubidium and potassium magneto-optical traps. *Phys. Rev. A* **73**, 013410 (2006). doi:10.1103/PhysRevA.73.013410

41. Y. R. P. Sortais, H. Marion, C. Tuchendler, A. M. Lance, M. Lamare, P. Fournet, C. Armellin, R. Mercier, G. Messin, A. Browaeys, P. Grangier, Diffraction-limited optics for single-atom manipulation. *Phys. Rev. A* **75**, 013406 (2007). doi:10.1103/PhysRevA.75.013406